

Accepted Manuscript

Meander anisotropic magnetoresistance bridge geomagnetic sensors

L.K. Quynh, B.D. Tu, N.T. Thuy, D.Q. Viet, N.H. Duc, A.T. Phung, D.T. Huong Giang

PII: S2468-2179(19)30102-9

DOI: <https://doi.org/10.1016/j.jsamd.2019.04.007>

Reference: JSAMD 224

To appear in: *Journal of Science: Advanced Materials and Devices*

Received Date: 23 March 2019

Revised Date: 22 April 2019

Accepted Date: 23 April 2019

Please cite this article as: L.K. Quynh, B.D. Tu, N.T. Thuy, D.Q. Viet, N.H. Duc, A.T. Phung, D.T.H. Giang, Meander anisotropic magnetoresistance bridge geomagnetic sensors, *Journal of Science: Advanced Materials and Devices*, <https://doi.org/10.1016/j.jsamd.2019.04.007>.

This is a PDF file of an unedited manuscript that has been accepted for publication. As a service to our customers we are providing this early version of the manuscript. The manuscript will undergo copyediting, typesetting, and review of the resulting proof before it is published in its final form. Please note that during the production process errors may be discovered which could affect the content, and all legal disclaimers that apply to the journal pertain.



Meander anisotropic magnetoresistance bridge geomagnetic sensors

L.K. Quynh^{1,2*}, B.D. Tu¹, N.T. Thuy¹, D.Q. Viet¹, N.H. Duc¹,
A.T. Phung³, and **D.T. Huong Giang**^{1*}

¹ Key Laboratory for Micro-nano Technology, VNU University of Engineering and Technology, Vietnam National University, Hanoi, 144 Xuan Thuy Road, Cau Giay, Hanoi, Vietnam

² Faculty of Physics, Hanoi Pedagogical University 2, Hanoi, Vietnam

³ Hanoi University of Science and Technology, Hanoi, Vietnam

* Corresponding authors: quynhkl@gmail.com; giangdth@vnu.edu.vn

Abstract

Anisotropic magnetoresistive (AMR) sensors have been useful since a long time for specific industrial applications. Their field detection sensitivity can be improved using magnetic flux concentrators to amplify the magnetic field strength sensed at the sensor. We demonstrate the design and fabrication of a micrometer-size meander AMR bridge sensor with an effective AMR branch length of 150. This sensor geometry exhibits a magnetic sensitivity as high as 1.25 mV/Oe (or 0.45 mV/V/Oe), which is an enhancement by a factor of about 300 compared to that of the corresponding simple AMR thin films. This opens a new challenge in the design and application of geomagnetic devices.

Keywords: Magnetic sensor, Anisotropic Magnetoresistance, Wheatstone bridge sensor, Geomagnetic devices, Permalloy.

Meander anisotropic magnetoresistance bridge geomagnetic sensors

L.K. Quynh^{1,2*}, B.D. Tu¹, N.T. Thuy¹, D.Q. Viet¹, N.H. Duc¹,
A.T. Phung³, and **D.T. Huong Giang**^{1*}

¹ Key Laboratory for Micro-nano Technology, VNU University of Engineering and Technology, Vietnam National University, Hanoi, 144 Xuan Thuy Road, Cau Giay, Hanoi, Vietnam

² Faculty of Physics, Hanoi Pedagogical University 2, Hanoi, Vietnam

³ Hanoi University of Science and Technology, Hanoi, Vietnam

* Corresponding authors: quynhkl@gmail.com; giangdth@vnu.edu.vn

Abstract

Anisotropic magnetoresistive (AMR) sensors have been useful since a long time for specific industrial applications. Their field detection sensitivity can be improved using magnetic flux concentrators to amplify the magnetic field strength sensed at the sensor. We demonstrate the design and fabrication of a micrometer-size meander AMR bridge sensor with an effective AMR branch length of 150. This sensor geometry exhibits a magnetic sensitivity as high as 1.25 mV/Oe (or 0.45 mV/V/Oe), which is an enhancement by a factor of about 300 compared to that of the corresponding simple AMR thin films. This opens a new challenge in the design and application of geomagnetic devices.

Keywords: Magnetic sensor, Anisotropic Magnetoresistance, Wheatstone bridge sensor, Geomagnetic devices, Permalloy.

1. Introduction

Although the development of diverse spintronics-based sensors has been intensively studied in the last three decades, the anisotropic magnetoresistive (AMR) sensors are still found useful for many specific industrial applications [1]. AMR sensors were primarily used as the reading heads in magnetic hard disk drivers. Thanks to their simple design, low cost, robustness and temperature stability, these sensors were developed for applications in the automotive and consumer electronics (*e.g.* for current or spatial position, speed and orientation angle as well as geomagnetic field sensing) or in bioengineering (*e.g.* for biomolecular detection or magnetic bead manipulation) *etc.*

Single-layer Ni-Fe films with the stoichiometric composition exhibit not only superior soft magnetic properties but also the controllable uniaxial magnetic anisotropy. Besides the material-nature magnetocrystalline, magnetoelastic anisotropies and the deposition-induced magnetic anisotropy effects, the shape anisotropy seems to be a simple geometrical parameter, which can be applied to create a single magnetic domain and a homogeneous internal magnetization oriented along the easy axis. By this approach, it was thought to be able to concentrate the residual magnetic flux density and thus, to well enhance the low magnetic field susceptibility in Metglas/PZT based sensors [2,3]. The stability, of the magnetic sensor output, in addition, must be ensured over a large range of temperatures and, in general, the signal to noise (S/N) ratio must be suppressed. These requirements are usually satisfactorily met thanks to the integration of the sensors in the Wheatstone bridge configuration, which can provide a null-voltage

output in the absence of an external stimulation field, while ensuring the same full output voltage of a single device [4-9, 11-13]. In order to get a higher voltage output, Wang et al. [14] purposed a Wheatstone bridge with barber pole structure. Practically, a classical Wheatstone bridge was designed based on typical 0° – 90° AMR magnetoresistors (see Fig. 1(a)) [4-7]. This bridge sensor exhibits a sensitivity as large as 2.15 mV/Oe (or 1.80 mV/V/Oe) corresponding to a magnetic detection limit better than 10^{-6} emu and hence is suitable for the detection of the superparamagnetic fluid of 50 nm- Fe_3O_4 -chitosan [5]. This makes the AMR bridge sensor fairly suitable for use as a biomedical detector.

Attempting to improve the field detection sensitivity using magnetic flux concentrators to amplify the magnetic field strength felt at the sensor, Henriksen *et al.* [8] and Persson [9] have developed meander planar Hall effect bridge (PHEB) sensors with varying length (l), width (w) and number (n) of AMR segments connecting in series in each branch (see Fig. 1(b)). They found that the sensor sensitivity is proportionally enhanced with the effective AMR branch length $l_{\text{eff}} (= (n \times l) / w)$ (hereafter simply referred to as effective length) and showed that it is possible to enhance the sensor output by a factor of 100 compared to that of cross shaped sensors made of the same magnetic stack [8-9]. In this geometry, however, the longer the l_{eff} the higher the total bridge resistance (R). Consequently, a Johnson (thermal, white, or Nyquist) noise ($S_J \sim TR$), which occurs in all magnetoresistors due to the random thermal motion of electrons, will rise at the temperature T [10].

To improve the sensor performance, not only the effective length and the equivalent resistance of the bridge but also the gap-distance between the AMR resistor segments must be optimized. Recently, we have developed several configurations of millimeter-size meander AMR bridge sensors for detecting magnetic nanoparticles [13]. There, the AMR resistors were connected not only in series, but also in series-parallel combination configurations (see *e.g.* Fig. 1(c)). In this article, a micrometer-size meander AMR bridge sensor with an effective length of 150 was designed and fabricated. The sensitivity of this sensor geometry has been enhanced by a factor of about 300 compared to that of the corresponding simple AMR sensors. The sensor exhibits a high potential application to sense the geomagnetic field direction.

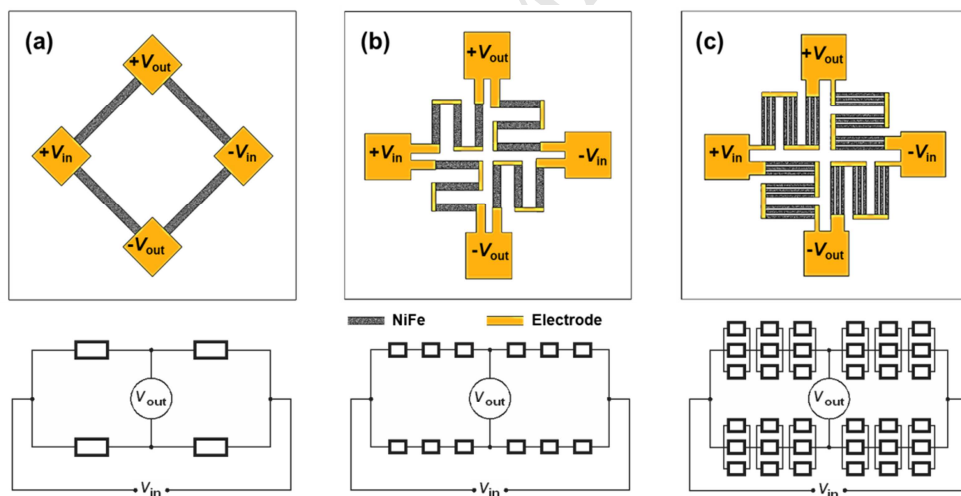


Fig. 1. Layout of the magnetic sensor geometry in the classic Wheatstone bridge: (a) single-magnetoresistor, (b) multi-magnetoresistors in series connection and (c) multi-magnetoresistors in combined series-parallel connection.

2. Experimental

Micrometer-size meander AMR bridge sensors were fabricated by combining the magnetron sputtering (*Model ATC 2000-F*) and lithography (*MJB4, Suss MicroTech*) techniques. Thin $\text{Ni}_{81.8}\text{Fe}_{18.2}$ films with the thickness ranging between 5 and 25 nm were deposited on thermally oxidized Si-wafers. A 5 nm-thick Ta layer was used both as buffer and capping one. The films were grown in an in-situ pinning magnetic field of $H_{\text{pin}} = 900$ Oe to establish the direction of the easy-axis anisotropy under a vacuum based pressure of 2.0×10^{-7} Torr and the Ar sputtering gas pressure of 2.2×10^{-3} Torr. The film crystal structure was characterized by mean of the X-Ray diffraction (XRD) using a D8 Discover (Bruker AXS GmbH). Images of the sensor configurations were recorded by the (optical) polarisation microscope (AX10 Scope A1 Carl Zeiss) and the scanning electron microscopy (SEM) namely the Nova NanoSEM 450 system.

Magnetic properties were investigated using the Lake Shore 7400 System vibration sample magnetometer (VSM). The room temperature resistance and magnetoresistance of both as-deposited films and sensor structures were measured using a *dc* four-terminal Keithley instrument arrangement. In the case of the sensor characterization, the input voltage V_{in} from the Keithley 6220 *dc* Precision Current Source was applied to the two opposite corners of the bridge and the voltage response V_{out} of the bridge was measured at the remaining two contacts as a function of the magnetic field applied in the film plane and perpendicular to the H_{pin} direction using a Keithley 2400 Multimeter. Samples were

tested in a homogeneous magnetic field up to 30 Oe created by a pair of Helmholtz coils of the type Lake Shore Model MH-2.5.

3. Results and discussion

3.1. Sensor design

The design of an efficient magnetic configuration for the sensor was elaborated using the finite element method with supports of the Maxwell 2D software (Ansys, Canonsburg, PA, USA). In this case, the magnetic flux density is an important parameter to investigate. Here, the measured magnetization (B - H) curve of a 5 nm-thick NiFe film was used to model the magnetic flux density distribution on each magnetoresistor segment. In this approach, the effective residual magnetic induction (residual flux density) B_{eff} (*i.e.* the magnetic induction after removing the applied magnetic field) is given by

$$B_{\text{eff}} = \frac{1}{V} \int_{\text{Volume}} B dV$$

3.1.1. Magnetic flux density in the single separated magnetoresistor segment

The magnetic flux concentration is defined by the uniaxial magnetic anisotropy. For real systems and objects, it could effectively be applied via the working point, which is related to the demagnetizing factor. As already mentioned, the enhancement of the magnetic flux density can be realized by increasing the effective length of magnetic samples (and/or objects). However, the concrete question is still open in detail for the length range, at which the efficiency can be reached. To solve this problem, here the

magnetic flux concentration was simulated as a function of the width of the magnetoresistive NiFe bars in the dimension variation of $l \times w \times t$ ($= 250 \mu\text{m} \times w \times 5 \text{ nm}$). The results are demonstrated in Fig. 2(a) and summarized in Fig. 2(b, c). It is clearly seen that, for narrow bars, *e.g.* for samples with the dimensions of $250 \mu\text{m} \times 10 \mu\text{m} \times 5 \text{ nm}$, the magnetic flux density almost reaches the theoretical value of the NiFe saturation magnetization (around 1 T) and distributes homogeneously along the sample length. For wide bars, *e.g.* for the sample with the dimension of $250 \mu\text{m} \times 50 \mu\text{m} \times 5 \text{ nm}$, however, the magnetic flux density is strongly reduced from the NiFe saturation magnetization and its inhomogeneity is decreased along the sample length. Moreover, the results reported in Fig. 2(b,c) also propose a critical range of $l_{\text{eff}} > 10$ for the effective length of the magnetic bars, at which the residual flux density, B_{eff} , approaches almost 95% of its saturation value.

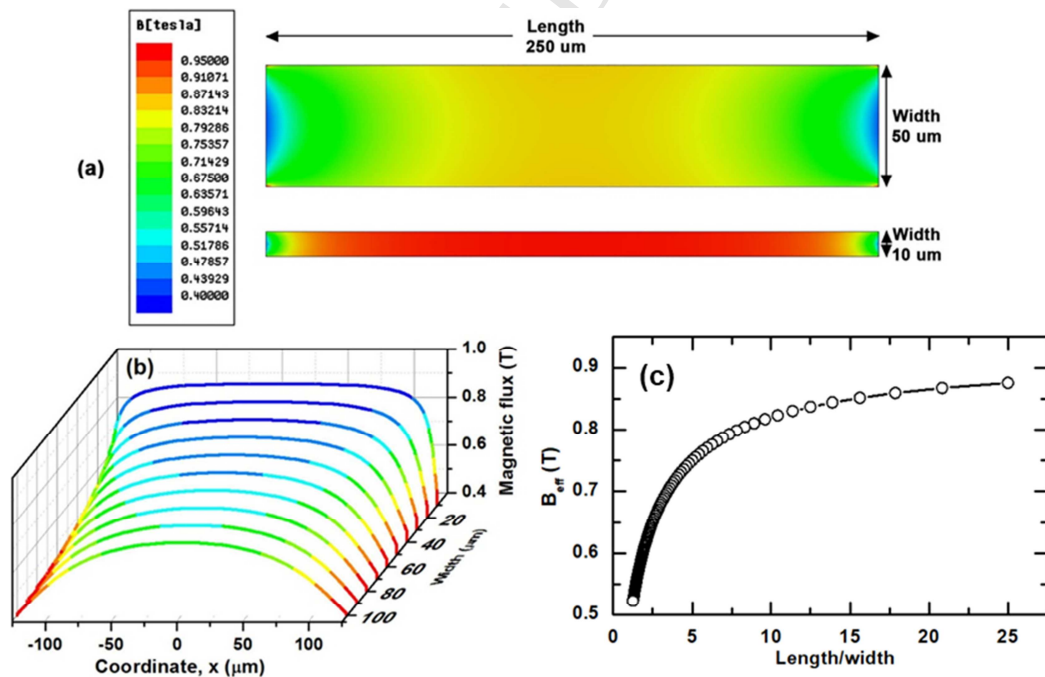


Fig. 2. The modeling results obtained for the 250 μm -length NiFe element with variable widths: the magnetic flux density distribution (a), the magnetic flux density data plotted along the length (b) and the effective residual magnetic flux density versus length/width ratio (c).

3.1.2. Magnetic flux density in the meander magnetoresistors

In meander magnetic systems, the magnetic flux density in each magnetoresistive segment is defined not only by its shape, but also by the stray magnetic fields created from the neighboring components. Let's consider a meander system consisting of three single magnetoresistive NiFe bars as illustrated in Fig. 3. By considering the results obtained for the magnetic bars in separated and combined configurations the followings are noted. Firstly, in the meander system, the residual magnetic flux density in the wide bars is strongly reduced in comparison to the corresponding single separated magnetoresistors (see Fig. 3(a,b)). In this case, highest magnetic flux density reaches only a value of about 0.71 T at the center of the 50 μm ×250 μm segment. Secondly, the magnetic flux density in the central bars (*i.e.* bar 2) is somewhat lower with respect to the bar at the edge sides (*e.g.* bar 1). Thirdly, these differences are enlarged at the narrow gap distances between the magnetoresistors, in particular, for the wide segments (Fig. 4). Indeed, due to the demagnetizing field contribution, B_{eff} is also decreased with the increasing number of the magnetoresistors placed close to each other and with the decreasing space between them. The modeling results show that the overall effective residual magnetic flux density reduces of about 17% and 28% when the gap-distance

decreases from $50\ \mu\text{m}$ to $20\ \mu\text{m}$ and $10\ \mu\text{m}$, respectively, for the magnetoresistors of $50\ \mu\text{m} \times 250\ \mu\text{m}$ in size, whereas, the corresponding values for the magnetoresistors of $10\ \mu\text{m} \times 250\ \mu\text{m}$ insize are only about 5% and 7%.

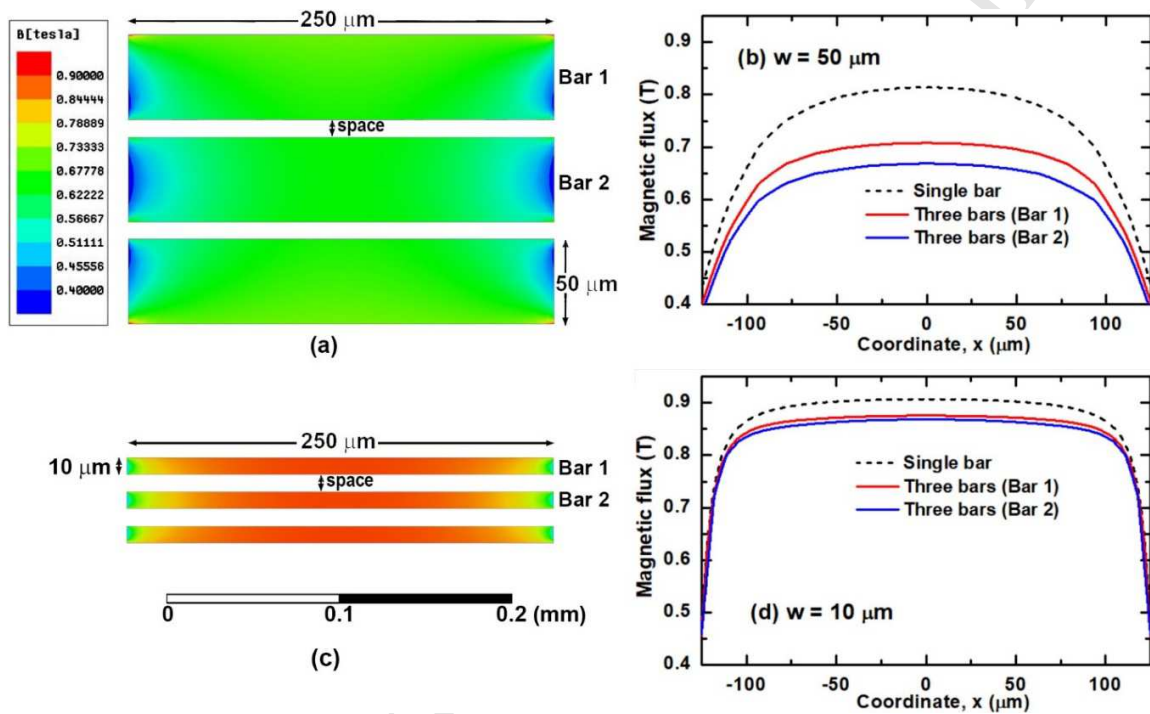


Fig. 3. Magnetic flux distribution and magnetic flux density data plotted along the center length in meander magnetoresistors in the geometical configuration consisting of three NiFe bars with dimensions of $50 \times 250\ \mu\text{m}^2$ (a,b) and $10 \times 250\ \mu\text{m}^2$ (c,d) placed at gap-distance of $10\ \mu\text{m}$.

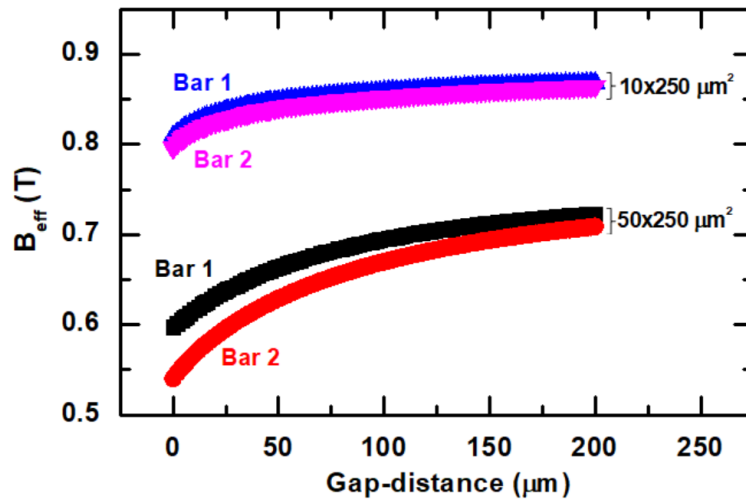


Fig. 4. The effective residual magnetic flux density versus gap-distance in meander magnetoresistors in the geometrical configuration consisting of 3 NiFe segments with dimensions of $50 \times 250 \mu\text{m}^2$ and $10 \times 250 \mu\text{m}^2$.

3.1.3. Bridge resistance

As already mentioned, the longer the effective length of the magnetoresistors the higher resistance and thus, the higher Johnson noise arises. In addition, for miniaturizing the Wheatstone bridge area a good arrangement of the resistor networks is desired. According to the simulation results, we can keep the AMR magnetoresistor with a high l_{eff} value. In such case, the effect of the gap-distance between the magnetoresistors can be reduced. However, in order to reduce the total bridge resistance and saving the sensor size, a combination of resistors in series-parallel connection is usually applied. Practically, all these factors will be applied for the realization of the real meander AMR bridge sensor, which will be presented below in subsection 3.2.2.

3.2. Real meander AMR bridge sensor

3.2.1. AMR materials characterization

Materials characterizations were undertaken on as-deposited $10 \times 10 \text{ mm}^2$ square NiFe films with different thicknesses of 5, 10, 15 and 20 nm. The XRD patterns of these samples are presented in Fig. 5 which indicate the formation of nanocrystallites in the films with thickness higher than 10 nm. By using the Scherrer method the grain size was estimated of about 10 nm. Similar results were reported in [15].

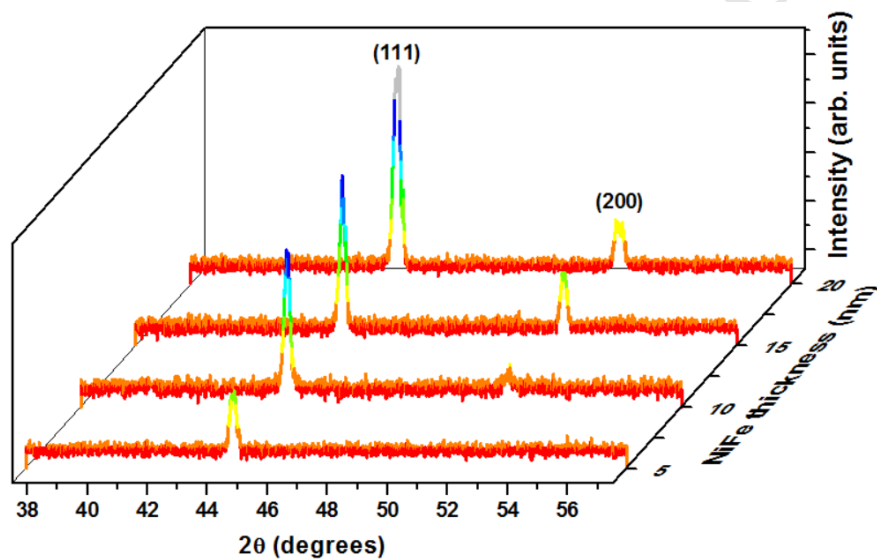


Fig. 5. X-ray diffraction patterns of NiFe films with different thickness.

A well-established in-plane uniaxial anisotropy is confirmed as illustrated in Fig. 6 by the magnetization loops measured in magnetic fields applied in-plane, both aligned along (EA) and perpendicular (HA) the pinned axis for the 5 nm-thick NiFe film. This behavior was also reported by [14]. This also suggests this film to be suitable for magnetic flux concentrator applications.

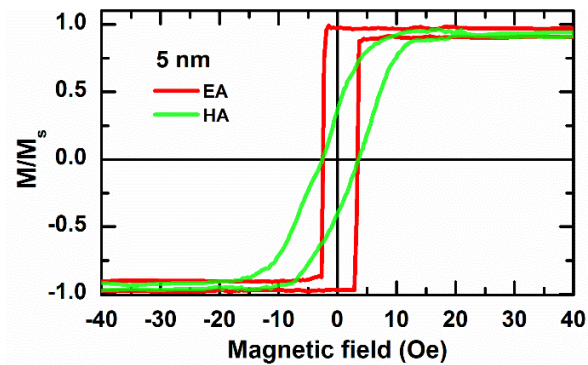


Fig. 6. Magnetization loops measured in magnetic fields applied in-plane, both aligned along (EA) and perpendicular (HA) the pinned axis for the NiFe sample of thickness of 5 nm.

Results of the magnetoresistance measurements also reveal the uniaxial magnetic anisotropy indicated from the magnetic measurements. Indeed, the voltage response and the AMR ratio measured along the pinning direction is rather weak. It is of about 25% of the AMR value measured in perpendicular direction (Fig. 7(a,b)). Unfortunately, among these films, the highest ratio of 0.23% was found for the 5 nm-thick NiFe film only (see Fig. 7(b)). In this case, the corresponding maximal magnetic field sensitivity dV/dH of 0.45×10^{-2} mV/Oe could be derived using an applied current of 1 mA (Fig. 7(c)). This thinnest film of 5 nm, hence, will be used in the real AMR bridge sensors as presented further below.

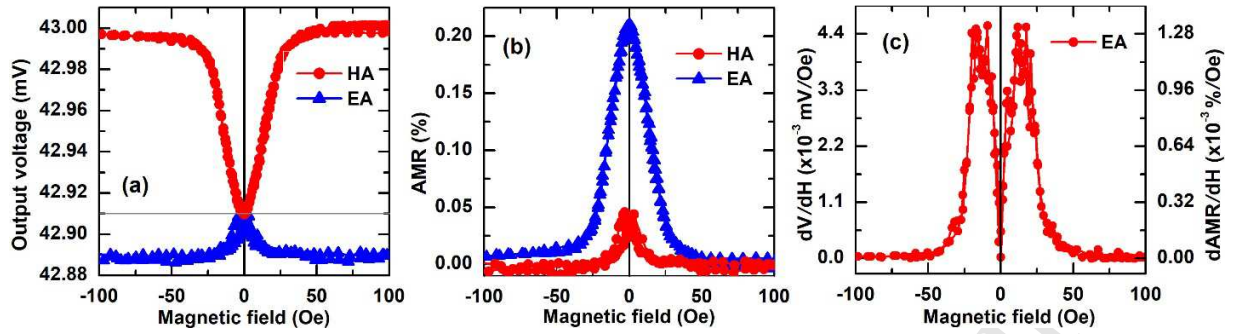


Fig. 7. The voltage response (a), anisotropic magnetoresistance AMR (b) and magnetic sensitivity of the voltage response dV/dH (c) measured in magnetic fields applied in-plane, both aligned along (EA) and perpendicular (HA) the pinned axis for the 5 nm-thick NiFe film.

3.2.2. Meander AMR bridge sensor

Following the simulation results, a meander AMR bridge sensor consisting of 18-magnetoresistors (with the size of $l \times w \times t = 250 \mu\text{m} \times 10 \mu\text{m} \times 5 \text{nm}$) connected in series-parallel combinations was fabricated. This geometrical configuration corresponds to the sensor with the effective length $l_{\text{eff}} = 150$. The four branches are arranged within a square of $2.5 \times 2.5 \text{cm}^2$. All junctions were deposited using Cu. The optical and scanning electron microscopic images of the as-fabricated sensor are shown in Fig. 8(a,b) and its equivalent resistance schema is illustrated in Fig. 8(c). The gap-distance between the magnetoresistance segments (*i.e.* segments parallelly connected) was kept at $10 \mu\text{m}$ and the gap-distance between the parallelly connected magnetoresistance blocks (*i.e.* the segment blocks serially connected) was of $20 \mu\text{m}$. The intrinsic resistance measured in

each branch yielded a value of 2.6 k Ω . As already predicted and pointed out from the simulation approach, this sensor configuration allows an optimal magnetic flux concentration.

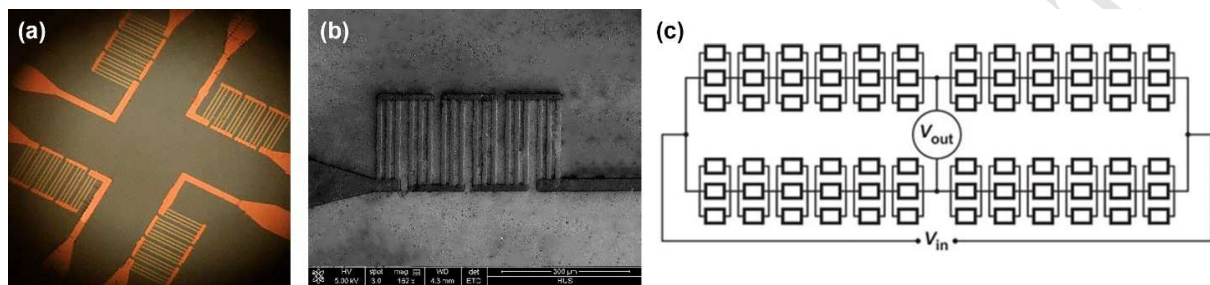


Fig. 8. Optical microscope (a) and Scanning electron microscope (b) images and the equivalent resistance schema (c) of the meander AMR bridge sensor under investigation.

Shown in Fig. 9 is the response signal of the meander AMR bridge sensor upon the external magnetic fields applied perpendicular to the pinning direction at the current of 5 mA. Clearly, the maximal voltage response and the magnetic sensitivity reach the values of about 49.7 mV and 7.36 mV/Oe at $H = 9$ Oe. Normalized to the applied measuring current of 1 mA, these values are reduced to 9.94 mV and 1.27 mV/Oe (or 0.45 mV/V/Oe) for ΔV and dV/dH , respectively. In comparison with the sensitivity reported for the millimeter-size meander AMR bridge sensors [13], this micrometer-size bridge sensor exhibits only the advantage in the total bridge resistance. However, it would be more useful to compare its performance with sensors of similar micrometer-size. In this case, as regard to the low field sensitivity of 0.45 mV/Oe reported for the meander PHE bridge sensor of the similar effective length ($l_{\text{eff}} = 140$) [8], the present meander AMR bridge sensor is almost 3 times more sensitive. In particular, it is here worthy to note that

there is the possibility to enhance the sensor sensitivity by a factor of 300 when considering the above mentioned magnetic sensitivity of the as-deposited AMR material. Moreover, this AMR bridge sensor exhibits also a better sensitivity with respect to that of 0.11 mV/V/Oe [11] 0.23 mV/V/Oe [12] obtained for spin valve-based magnetoresistance bridge sensors.

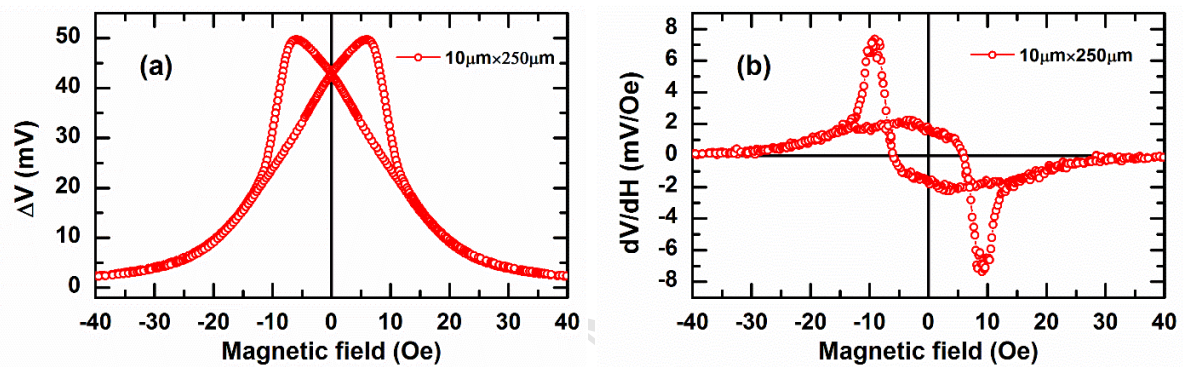


Fig. 9. Magnetic field response of the sensor signal ΔV (a) and magnetic susceptibility dV/dH (b) for the meander AMR Wheatstone bridge sensor measured at current of 5 mA.

3.2.3. Geomagnetic devices

For practical applications for the local orientation and positioning in the human lives, the strength as well as the direction of the terrestrial magnetic fields are sensed and measured by geomagnetic devices. Geomagnetic sensing devices must be particularly sensitive to be utilizable for the determination of the spatial azimuth and pitch angles. For the purposes of developing such devices, different two dimensional (2-D) and three-dimensional (3-D) magnetic sensors were proposed for magnetoelectric Metglas/PZT

based sensors [2,3] The one dimensional (1-D) configuration in this investigation, however, can demonstrate a test approach for revealing the actual sensor sensitivity.

For the orientation angle dependence test of the sensor, the meander AMR bridge sensor is always integrated to a Helmholtz coil for anchoring on a fixed working bias field of 9 Oe. The terrestrial magnetic field strength (H_{earth}) in the horizontal plane was sensed by fully rotating the sensor system in the horizontal plane about the vertical axis while the response signal, *i.e.* the output voltage of the sensor was recorded in the measurement system. The experimental results are presented in Fig. 10. It is clearly to see that the recorded signal is well fitted with the harmonic cosine function of the rotation φ -angle between H_{bias} and H_{earth} . The (azimuth) angle sensitivity of the sensor can be determined from the highest slope of this cosine curve and a value as high as 36 $\mu\text{V}/\text{degree}$ has been derived. This result suggests an excellent possibility to use this 1-D meander AMR bridge sensor to develop a 2-D sensor configuration which can serve as an electronic compass towards spatial navigation.

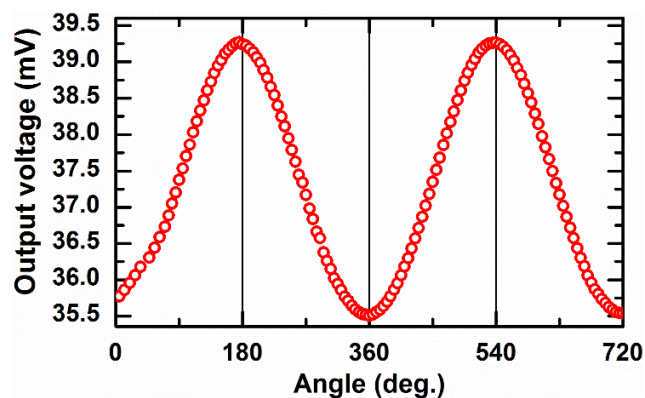
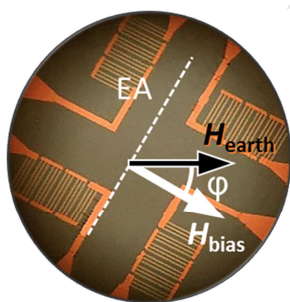


Fig. 10. Experimental setup (a) and the response signal (b) of the meander AMR bridge sensor as a function of the azimuth angle in the terrestrial magnetic field.

4. Conclusion

We have successfully designed and fabricated a micrometer-size meander AMR bridge sensor consisting of 18 segments of 5 nm-thick NiFe magnetoresistors intergrated in series-parallel connecting networks with an effective length of 150. This sensor configuration can improve the magnetic flux concentration to amplify the magnetic field strength felt at the sensor and thus significantly enhance the field detection sensitivity. This sensor geometrical configuration exhibits a magnetic sensitivity as high as 1.25 mV/Oe (or 0,45 mV/V/Oe) and an enhancement of the sensitivity by a factor of about 300 compared to corresponding simple AMR sensors. With an orientation angle sensitivity as high as 36 μ V/degree, this sensor is highly potential for application in geomagnetic devices.

Acknowledgment

This work was supported by Vietnam National University, Hanoi under the Research Project No. QG 16.89.

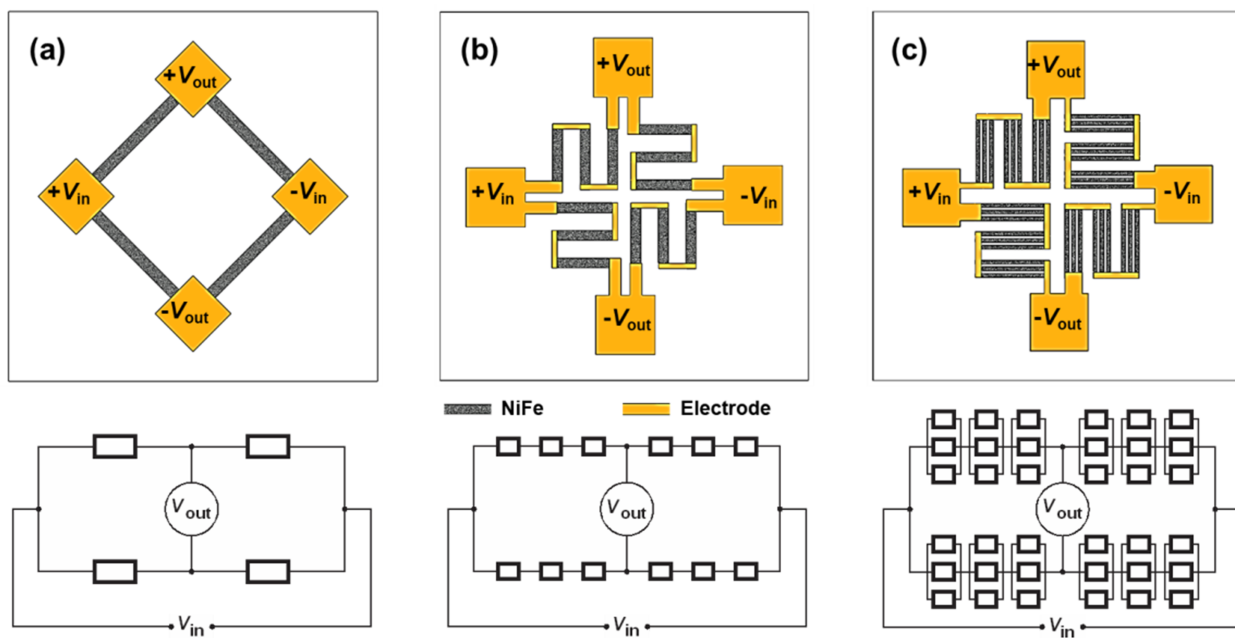
References

1. L. Jogschies, D. Klaas, R. Kruppe, J. Rittinger, P. Taptimthong, A. Wienecke, M. Wurz, Recent Developments of Magnetoresistive Sensors for Industrial Applications, *Sensors* 15 (2015) 28665.
2. D.T. Huong Giang, P.A. Duc, N.T. Ngoc and N.H. Duc, Geomagnetic sensors based on Metglas/PZT laminates, *Sensor and Actuator A: Physical* 179 (2012) 78.
3. N.H. Duc, B.D. Tu, N.T. Ngoc, V.D. Lap and D.T. Huong Giang, Metglas/PZT-Magnetolectric 2-D Geomagnetic Device for Computing Precise Angular Position, *IEEE Transactions on Magnetics* 49 (2013) 4839.
4. Michael J. Haji-Sheikh and Young Yoo, An accurate model of a highly ordered 81/19 Permalloy AMR Wheatstone bridge sensor against a 48 pole pair ring-magnet, *Int. J. Intelligent Systems Technologies and Applications* 3 (2007) 95.
5. L.K. Quynh, B.D. Tu, D.X. Dang, D.Q. Viet, L.T. Hien, D.T. Huong Giang and N.H. Duc, Detection of magnetic nanoparticles using simple AMR sensors in Wheatstone bridge, *J. of Sci: Adv. Mater. Devices*, 1 (2016) 98-102.
6. Anders Dahl Henriksen, Giovanni Rizzi, Frederik Westergaard Østerberg, Mikkel Fougth Hansen, Optimization of magnetoresistive sensor current for on-chip magnetic bead detection using the sensor self-field, *Journal of Magnetism and Magnetic Materials* 380 (2015) 209-214.

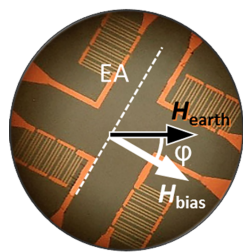
7. C. Wang, W. Su, Z. Hu, J. Pu, M. Guan, B. Peng, W. Ren, Z. Zhou, M. Liu, Highly Sensitive Magnetic Sensor Based on Anisotropic Magnetoresistance Effect, *IEEE Transactions on Magnetics* 54 (2018) 2301103.
8. A.D. Henriksen, B.T. Dalslet, D.H. Skieller, K.H. Lee, F. Okkels, M.F. Hansen, Planar Hall effect bridge magnetic field sensors, *Appl. Phys. Lett.* 97 (2010) 013507.
9. A. Persson, R.S. Bejhed, H. Nguyen, K. Gunnarsson, B.T. Dalslet, F.W. Østerberg, Low-frequency noise in planar Hall effect bridge sensors, *Sensors and Actuators A* 171 (2011) 212 – 218.
10. J.B. Johnson, Thermal agitation of electricity in conductors, *Nature* 20 (1927) 119.
11. S. Yan, Z. Cao, Z. Guo, Z. Zheng, A. Cao, Y. Qi, Q. Leng, W. Zhao, Design and fabrication of full wheatstone- bridge-based angular GMR sensors, *Sensors (Switzerland)* 18 (2018) 1832.
12. V.S. Luong, A.T. Nguyen, T.H.D. Tran , Antiparallel-pinned spin valves with modified artificial antiferromagnetic layer for full-bridge magnetic sensors, *IEEE Transactions on Magnetics*, 54 (2018) 8415772.
13. L.K. Quynh, B.D. Tu, C.V. Anh, N.H. Duc, A.T. Phung, T.T. Dung and D.T. Huong Giang, Design Optimization of an Anisotropic Magnetoresistance Sensor for Detection of Magnetic Nanoparticles *J. Electronic Materials*, 48(2) (2019) 997-1004.
14. Chenying Wang, Wei Su, Zhongqiang Hu, Jiangtao Pu, Mengmeng Guan, Bin Peng, Lei Li, Wei Ren, Ziyao Zhou, Zhuangde Jiang and Ming Liu, Highly Sensitive

Magnetic Sensor Based on Anisotropic Magnetoresistance Effect, IEEE Transactions on Magnetics, 54 (2018) 2301103

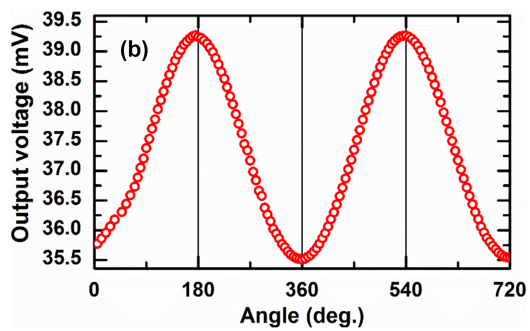
15. O. Alves Santos, R. L. Rodríguez-Suárez, A. Azevedo, S. M. Rezende and F. Bohn, Thickness dependence of the magnetic anisotropy and dynamic magnetic response of ferromagnetic NiFe films, J. Phys. D: Appl. Phys. 50 (2017) 185001.



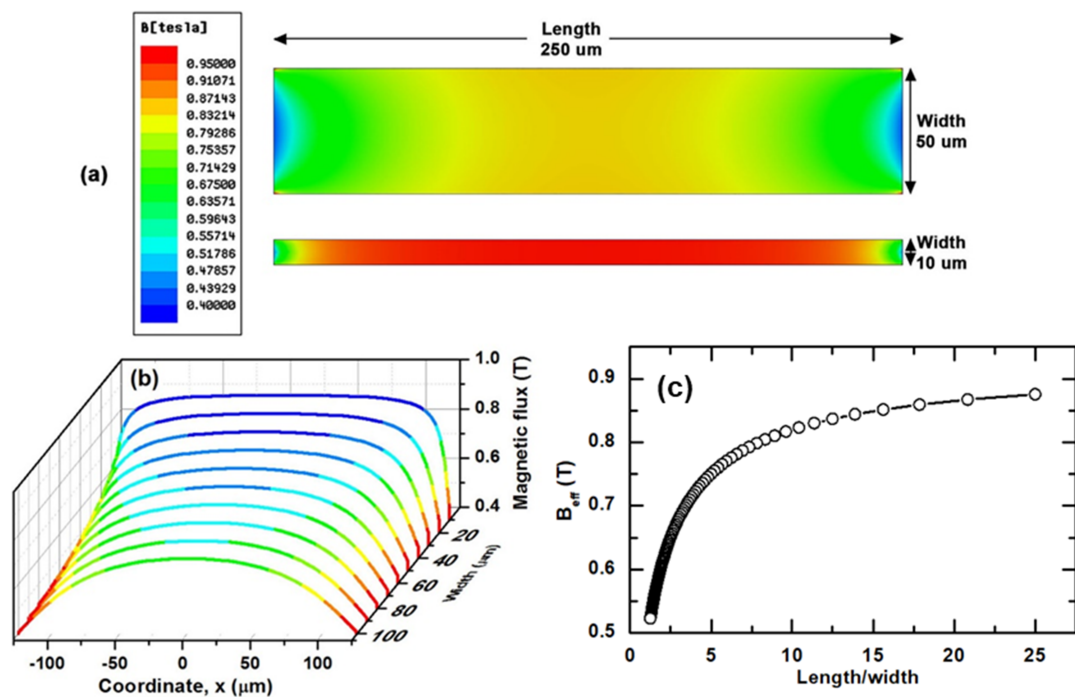
ACCEPTED MANUSCRIPT

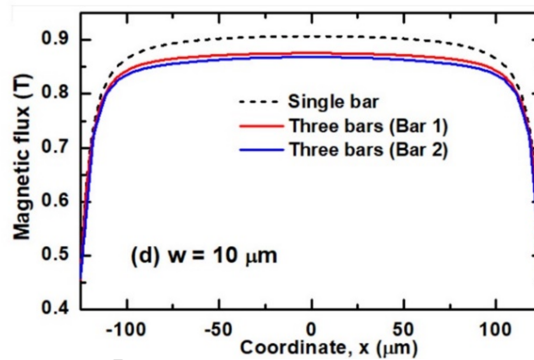
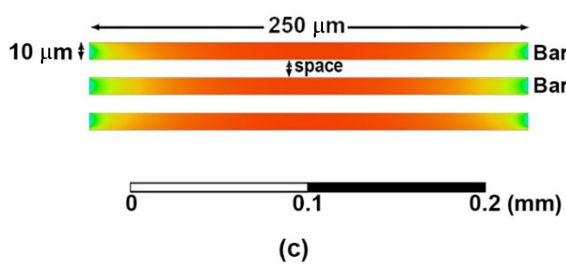
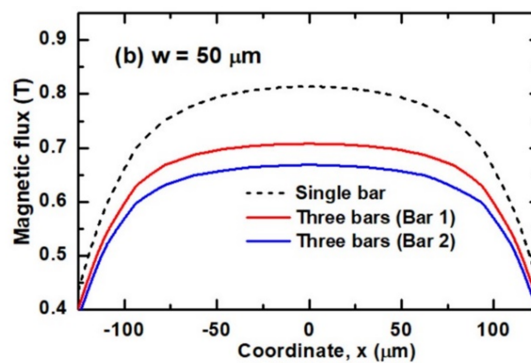
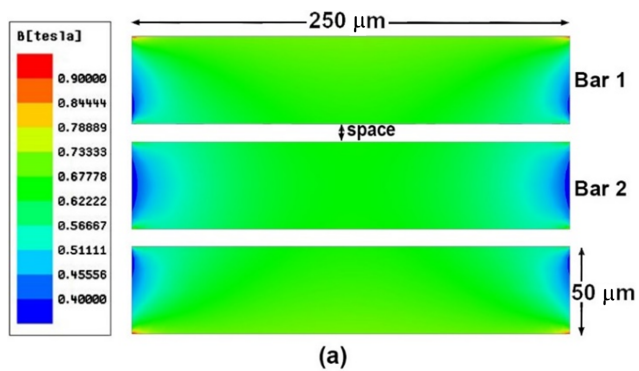


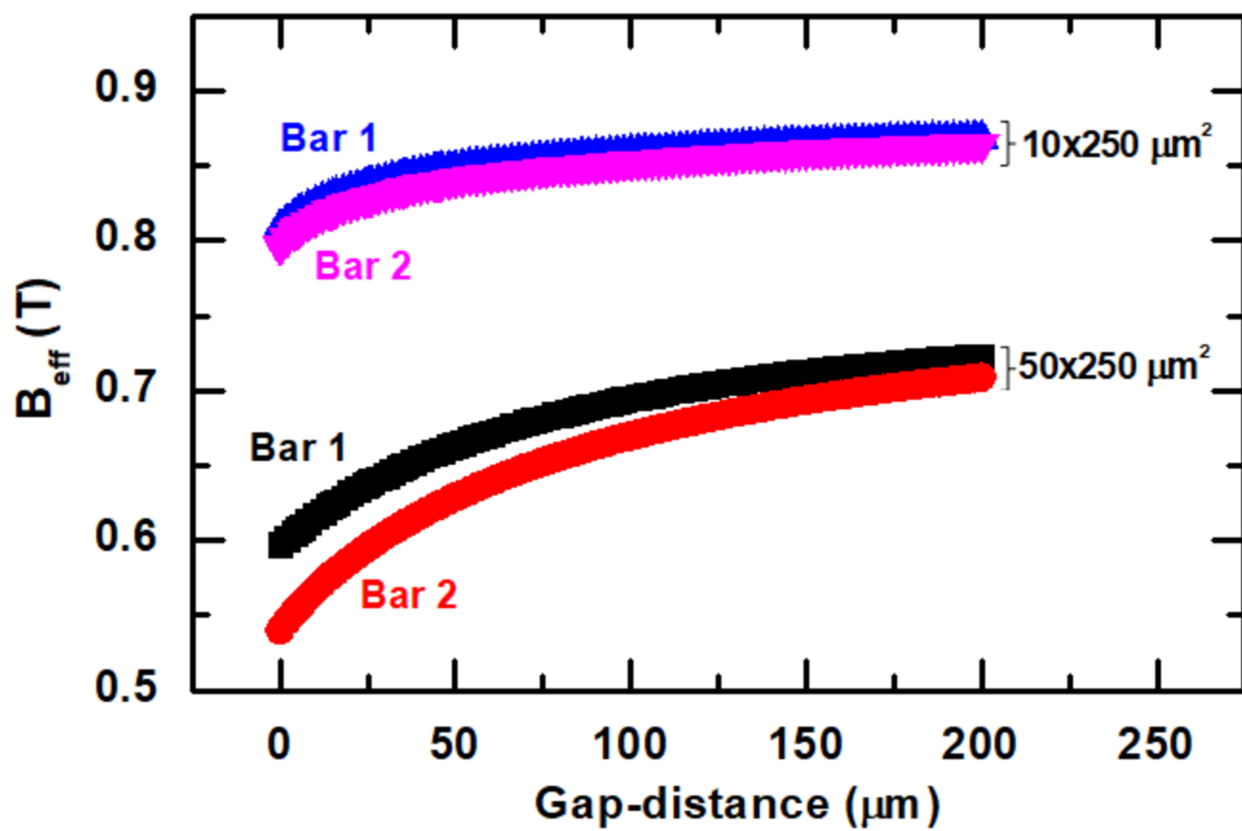
(a)

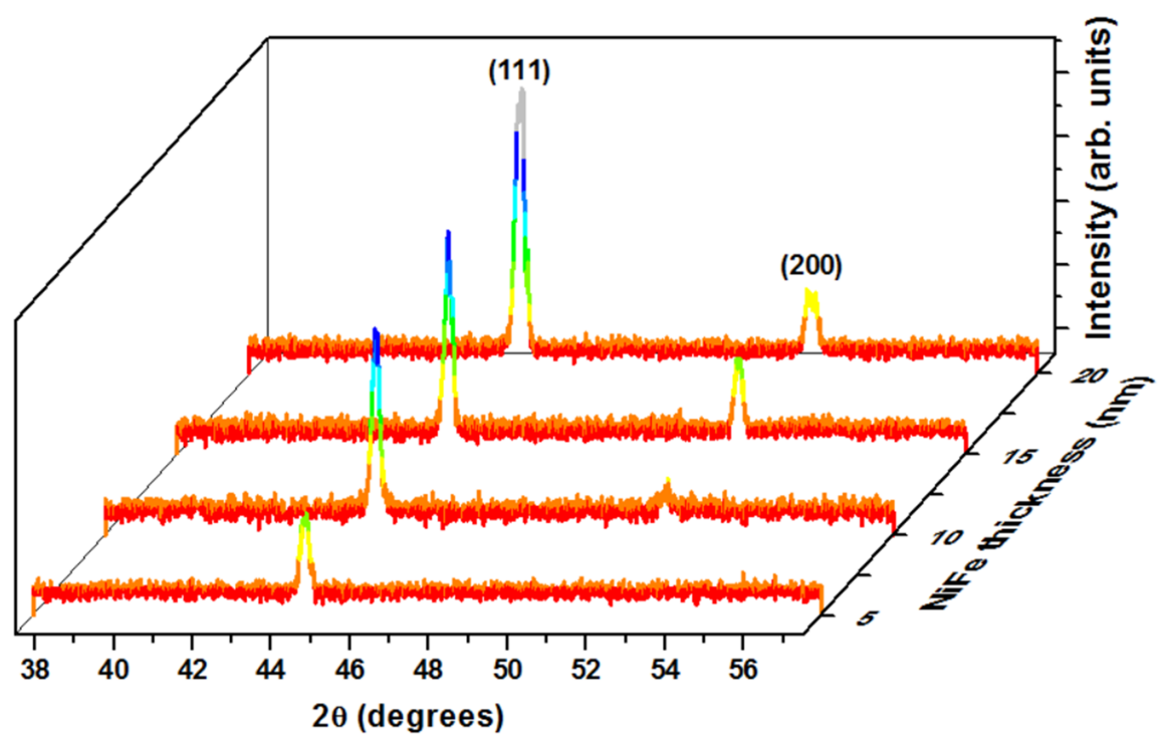


ACCEPTED MANUSCRIPT

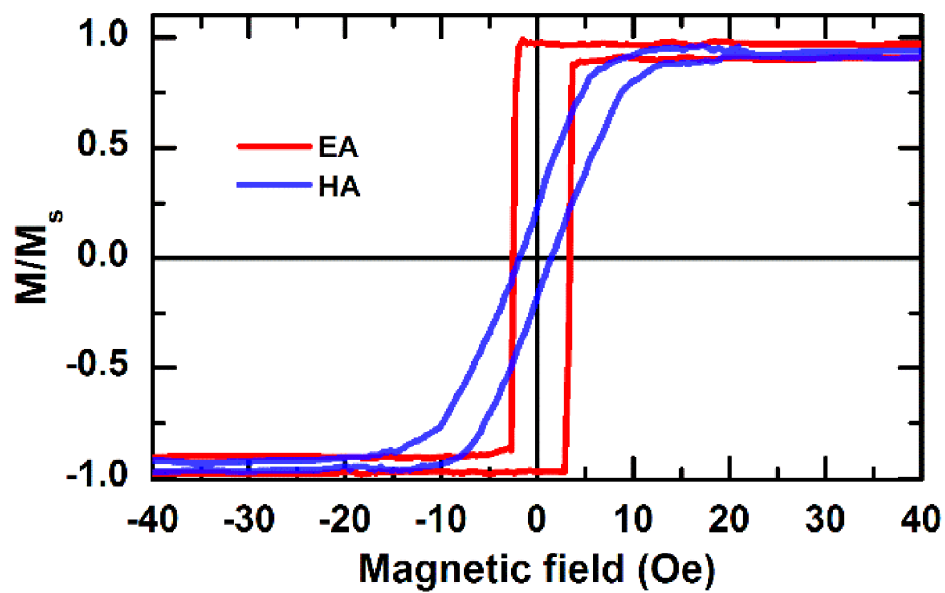


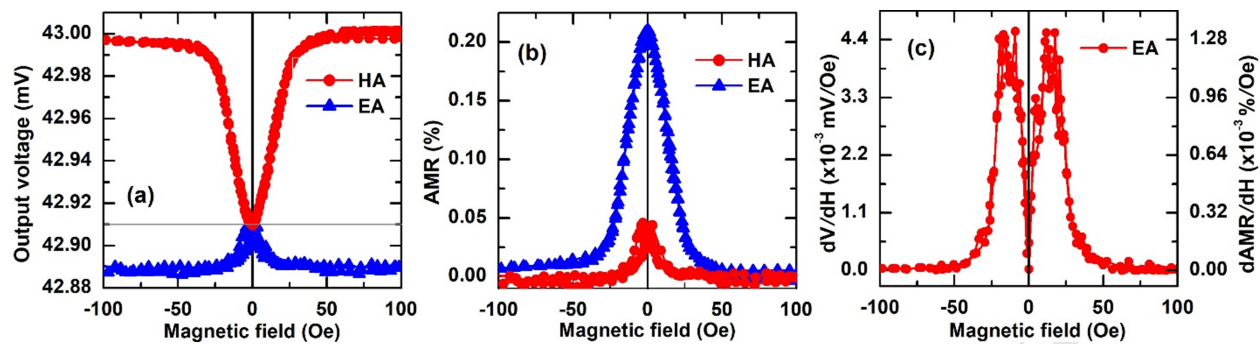


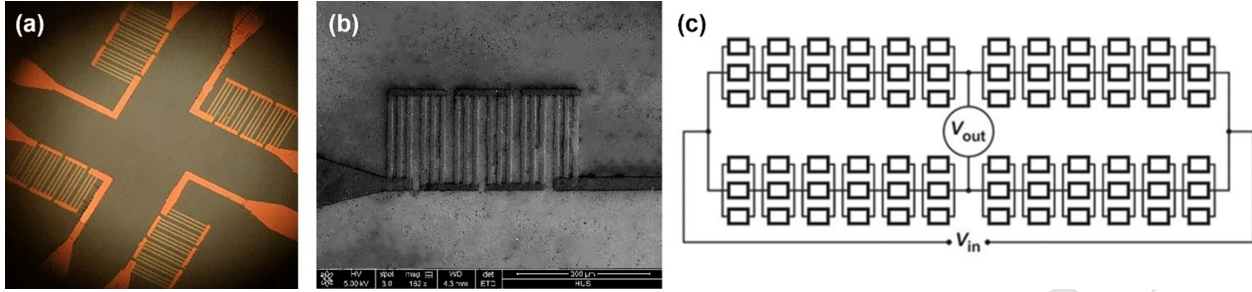




ACCEPTED MANUSCRIPT







ACCEPTED MANUSCRIPT

